Computer Physics Communications 185 (2014) 2903–2912

Contents lists available at ScienceDirect

Computer Physics Communications

journal homepage: www.elsevier.com/locate/cpc

Collisions of electrons with hydrogen atoms II. Low-energy program using the method of the exterior complex scaling☆

Jakub Benda *, Karel Houfek

Institute of Theoretical Physics, Faculty of Mathematics and Physics, Charles University in Prague, V Holešovičkách 2, Prague, Czech Republic

ARTICLE INFO

Article history:
Received 28 January 2014
Received in revised form
20 May 2014
Accepted 26 May 2014
Available online 11 June 2014

Keywords:
Electron–hydrogen scattering
Exterior complex scaling

ABSTRACT

While collisions of electrons with hydrogen atoms pose a well studied and in some sense closed problem, there is still no free computer code ready for "production use", that would enable applied researchers to generate necessary data for arbitrary impact energies and scattering transitions directly if absent in on-line scattering databases. This is the second article on the Hex program package, which describes a new computer code that is, with a little setup, capable of solving the scattering equations for energies ranging from a fraction of the ionization threshold to approximately 100 eV or more, depending on the available computational resources. The program implements the exterior complex scaling method in the B-spline basis.

Program summary

Program title: hex-ecs

Catalogue identifier: AETI_v1_0

Program summary URL: http://cpc.cs.qub.ac.uk/summaries/AETI_v1_0.html

Program obtainable from: CPC Program Library, Queen's University, Belfast, N. Ireland

Licensing provisions: Standard CPC licence, http://cpc.cs.qub.ac.uk/licence/licence.html

No. of lines in distributed program, including test data, etc.: 44 440

No. of bytes in distributed program, including test data, etc.: 322 643

Distribution format: tar.gz

Programming language: C++11.

Computer: Any.

Operating system: Any system with a C++11 compiler (e.g. GCC 4.8.1; tested on OpenSUSE 13.1 and Windows 8).

Has the code been vectorized or parallelized?: Parallelized by OpenMP and MPI.

RAM: Depending on input; 4.9 GiB for the test run.

Classification: 2.4.

External routines: GSL [1], HDF5 [2], UMFPACK [3], FFTW3 [4], optionally with OpenBLAS [5].

Nature of problem:
Solution of the two-particle Schrödinger equation in central field.

Solution method:
The two-electron states are expanded into angular momentum eigenstates, which gives rise to the coupled bi-radial equations. The bi-radially dependent solution is then represented in a B-spline basis, which transforms the set of equations into a large matrix equation in this basis. The boundary condition is of Dirichlet type, thanks to the use of the exterior complex scaling method, which extends the coordinates into the complex plane. The matrix equation is then solved by preconditioned conjugate gradients.

☆ This paper and its associated computer program are available via the Computer Physics Communication homepage on ScienceDirect (http://www.sciencedirect.com/science/journal/00104655).

* Corresponding author. Tel.: +420 723716589.
E-mail addresses: jakub.benda@seznam.cz (J. Benda), karel.houfek@mff.cuni.cz (K. Houfek).

http://dx.doi.org/10.1016/j.cpc.2014.05.021

Running time:
Depending on input; 16 min for the test run on Intel i3 3.07 GHz processor (2 threads).

References:

[1] M. Galassi, et al., GNU Scientific Library: Reference Manual, Network Theory Ltd., 2003.
[2] The HDF Group, Hierarchical Data Format, version 5 (1997–2014), http://www.hdfgroup.org/HDF5/.
[3] T. A. Davis, ACM Trans. Math. Softw. 30 (2004) 196–199.
[4] M. Frigo, Steven, G. Johnson, Proceedings of the IEEE (2005) 216–231.
[5] Z. Xianyi, W. Qian, Z. Yunquan, 2012 IEEE 18th International Conference on Parallel and Distributed Systems (ICPADS), 17–19 Dec. 2012.

1. Introduction

This paper presents to our knowledge the first release of a computer code aimed at the solution of electron–hydrogen scattering that is based on the exterior complex scaling method (see e.g. the recent review by Bray et al. [1]). The code is a part of a larger project called Hex consisting of several programs that implement different methods based on quantum mechanics. The ultimate goal of the project is to cover all physically relevant energies and processes that occur during the electron–hydrogen scattering. The scope is non-relativistic at the moment, but extension to relativistic effects is expected to be done in the future. This program is aimed at low and intermediate energies, from a fractions of electronvolt to several times the ionization threshold. Other programs of the package use different methods that are valid just for higher energies. Each of these programs produces a unified output that is expected to be merged into a single database and together with both an on-line and off-line interface provided for further use by other researchers. The database interface hex-db and the high-energy code hex-dwba are described in the first paper of this series.

2. Theory

The theory closely follows the review article by Bartlett [2]. We use atomic units throughout, that is $\hbar = m_e = e = 4\pi\epsilon_0 = 1$ and $c = 1/\alpha \sim 137$.

The Schrödinger equation

$$(E - \hat{H}_{\text{full}})\Psi^S = 0 \tag{1}$$

for a state with a given spin S can be recast into a "scattering form" using the formulas $\Psi^S = \Psi_i^S + \Psi_{\text{sc}}^S$ and $(\hat{H}_{\text{full}} - \hat{H}_{\text{int}} - E)\Psi_i^S = 0$, so that

$$(E - \hat{H}_{\text{full}})\Psi_{\text{sc}}^S = \hat{H}_{\text{int}}\Psi_i^S, \tag{2}$$

where the full hamiltonian $\hat{H}_{\text{full}}$ is

$$\hat{H}_{\text{full}} = \hat{H}_1 + \hat{H}_2 + V_{12}, \qquad \hat{H}_j = -\frac{\nabla_j^2}{2} - \frac{1}{r_j}, \qquad V_{12} = \frac{1}{|\boldsymbol{r}_1 - \boldsymbol{r}_2|} \tag{3}$$

and the interaction hamiltonian $\hat{H}_{\text{int}}$ contains potentials acting on the projectile: the Coulomb force of the proton and of the other electron. This is either

$$\hat{H}_{\text{int}} = V_{12} - \frac{1}{r_1} \tag{4}$$

or the same expression with the indices interchanged, $1 \leftrightarrow 2$, depending on the identification of the electrons in the initial state Ψ_i^S (projectile/atomic electron). The separation of states with different spin is possible, thanks to the absence of spin-dependent terms in the non-relativistic hamiltonian. See the previous paper for a detailed discussion on the importance of relativistic corrections. The only dependence on (total) spin is contained in the anti/symmetrization of the initial state.

Eq. (2) is accompanied by the scattering boundary condition, which has different forms for discrete and for continuum processes. In the case of elastic scattering or excitation, the required asymptotic behavior is

$$\Psi_{\text{sc}}^S(\boldsymbol{r}_1, \boldsymbol{r}_2) \underset{r_2/r_1 \to 0}{\overset{r_1 \to \infty}{\longrightarrow}} \sum_j f_j(\hat{\boldsymbol{k}}_j)\frac{\mathrm{e}^{\mathrm{i}k_j r_1}}{r_1}P_j(\boldsymbol{r}_2), \tag{5}$$

$$\Psi_{\text{sc}}^S(\boldsymbol{r}_1, \boldsymbol{r}_2) \underset{r_1/r_2 \to 0}{\overset{r_2 \to \infty}{\longrightarrow}} \sum_j f_j(\hat{\boldsymbol{k}}_j)\frac{\mathrm{e}^{\mathrm{i}k_j r_2}}{r_2}P_j(\boldsymbol{r}_1). \tag{6}$$

Here j denotes the scattering channels (different hydrogen excitations), f_j is the scattering amplitude of transition to the jth channel from the initial state, $\boldsymbol{k}_j$ is the outgoing electron momentum and P_j is the channel function (hydrogenic orbital). In the case of ionization the asymptotic form of the scattering state can be expressed using the Coulomb waves

$$\phi_j = \Gamma(1 - \mathrm{i}\alpha_j)\mathrm{e}^{-\frac{1}{2}\pi\alpha_j}{}_1F_1(\mathrm{i}\alpha_j;\, 1;\, -\mathrm{i}(k_j r_j + \boldsymbol{k}_j \cdot \boldsymbol{r}_j)) \tag{7}$$

as a product [3]

$$\Psi_{\text{sc}}^S(\boldsymbol{r}_1, \boldsymbol{r}_2) \overset{r_1, r_2 \to \infty}{\longrightarrow} \frac{1}{(2\pi)^3}\mathrm{e}^{\mathrm{i}\boldsymbol{k}_1 \cdot \boldsymbol{r}_1}\mathrm{e}^{\mathrm{i}\boldsymbol{k}_2 \cdot \boldsymbol{r}_2}\phi_1\phi_2\phi_{12}. \tag{8}$$

The important factors for the method of exterior complex scaling used in this work are the complex exponentials. See [3] for more details and definition of α_j and the special functions contained in the formula (7).

Next, the solution is expanded as

$$\Psi_{\text{sc}}^S(\boldsymbol{r}_1, \boldsymbol{r}_2) = \frac{1}{r_1 r_2}\sum_{LM\ell_1\ell_2} \psi_{\ell_1\ell_2}^{LMS}(r_1, r_2)\mathcal{Y}_{\ell_1\ell_2}^{LM}(\hat{\boldsymbol{r}}_1, \hat{\boldsymbol{r}}_2), \tag{9}$$

where the bi-polar spherical functions $\mathcal{Y}_{\ell_1\ell_2}^{LM}$ are defined as a combination of the spherical functions Y_l^m [4, Section 6.7] and Clebsch–Gordan coefficients $C_{l_1 m_1 l_2 m_2}^{LM}$ [5, Section 27.9],

$$\mathcal{Y}_{\ell_1\ell_2}^{LM}(\hat{\boldsymbol{r}}_1, \hat{\boldsymbol{r}}_2) = \sum_{m=-\ell_1}^{\ell_1} C_{\ell_1 m \ell_2 M-m}^{LM} Y_{\ell_1}^m(\hat{\boldsymbol{r}}_1)Y_{\ell_2}^{M-m}(\hat{\boldsymbol{r}}_2), \tag{10}$$

and are the eigenfunctions of the square of the total angular momentum $\hat{L}^2$, its third component $\hat{L}_z$ and the squares of the angular momenta of each electron $\hat{L}_1^2$, $\hat{L}_2^2$. The spin is treated separately from the angular momentum L because no relevant coupling terms exist in the non-relativistic hamiltonian given by (3). There will be an independent solution ("partial wave") for every allowed

combination of the conserved global quantum numbers L, M, S and Π, where Π is the parity of the state. The two parities are also not coupled by hamiltonian (3). Every such function solves the set of bi-radial equations

$$\left(E-\hat{H}_1-\hat{H}_2\right)\psi^{LMS\Pi}_{\ell_1\ell_2}-\sum_{\ell_1'\ell_2'}\left\langle \mathcal{Y}^{LM}_{\ell_1\ell_2}\right| V_{12}\left|\mathcal{Y}^{LM}_{\ell_1'\ell_2'}\right\rangle \psi^{LMS\Pi}_{\ell_1'\ell_2'} = \chi^{LMS\Pi}_{\ell_1\ell_2} \tag{11}$$

obtained from (2) by projecting on a coupled spherical function $\mathcal{Y}^{LM}_{\ell_1\ell_2}$. The order of this set of equations is given by all the possible values of ℓ_1 and ℓ_2 satisfying

$$|\ell_1-\ell_2|\le L\le \ell_1+\ell_2, \tag{12}$$

but in practice this set is truncated. The truncation is controlled by an integer parameter n_L introduced by Bartlett [2]; the set of (ℓ_1,ℓ_2) pairs allowed by (12) is further restricted by the relation

$$L\le \ell_1+\ell_2\le L+n_L. \tag{13}$$

The convergence is achieved by raising the value of n_L to include a sufficient amount of angular momenta.

The matrix element of the two-electron potential can be expressed in a multipole expansion

$$\left\langle \mathcal{Y}^{LM}_{\ell_1\ell_2}\right| V_{12}\left|\mathcal{Y}^{L'M'}_{\ell_1'\ell_2'}\right\rangle = \delta_{LL'}\delta_{MM'}\,\langle \ell_1\ell_2||V_{12}||\ell_1'\ell_2'\rangle_L\,, \tag{14}$$

where

$$\langle l_1l_2||V_{12}||l_3l_4\rangle_L=\sum_\lambda f^\lambda_{l_1l_2l_3l_4;L}\frac{r^\lambda_<}{r^{\lambda+1}_>} \tag{15}$$

is the *reduced matrix element* of the inter-electron interaction potential. The summation runs over all λ-s allowed by the explicit form of f^λ:

$$f^\lambda_{\ell_1\ell_2\ell_1'\ell_2';L}=(-1)^{L+\ell_2+\ell_2'}[\ell_1\ell_2\ell_1'\ell_2']\begin{Bmatrix}\ell_1 & \ell_2 & L\\ \ell_2' & \ell_1' & \lambda\end{Bmatrix}\times\begin{pmatrix}\ell_1 & \lambda & \ell_1'\\ 0 & 0 & 0\end{pmatrix}\begin{pmatrix}\ell_2 & \lambda & \ell_2'\\ 0 & 0 & 0\end{pmatrix}, \tag{16}$$

where $[\ell_1\ell_2\ell_1'\ell_2']\equiv\sqrt{(2\ell_1+1)(2\ell_2+1)(2\ell_1'+1)(2\ell_2'+1)}$, parentheses denote the Wigner 3j-symbol [6, Section 3.7] and the braces the 6j-symbol [6, Section 6.1].

The right-hand side of Eq. (11) has the form

$$\chi^{LMS\Pi}_{\ell_1\ell_2}(r_1,r_2)=\frac{2}{k_i}\sum_l\sqrt{4\pi(2l+1)}C^{LM}_{l_im_i l0}\mathrm{i}^l\times\left(\chi^{(1)L}_{\ell_1\ell_2 l}(r_1,r_2)+(-1)^{L+S+\ell_1+\ell_2}\chi^{(2)L}_{\ell_1\ell_2 l}(r_1,r_2)\right), \tag{17}$$

$$\chi^{(1)L}_{\ell_1\ell_2 l}(r_1,r_2)=\left(\langle l_1l_2||V_{12}||l_il\rangle_L-\frac{1}{r_2}\delta^{l_i}_{l_1}\delta^{l}_{l_2}\right)P_{n_il_i}(r_1)\hat{j}_l(k_ir_2), \tag{18}$$

$$\chi^{(2)L}_{\ell_1\ell_2 l}(r_1,r_2)=\left(\langle l_1l_2||V_{12}||ll_i\rangle_L-\frac{1}{r_2}\delta^{l}_{l_1}\delta^{l_i}_{l_2}\right)\hat{j}_l(k_ir_1)P_{n_il_i}(r_2). \tag{19}$$

In the above lines, the original incoming wave function

$$\Psi_i(\boldsymbol{r}_1,\boldsymbol{r}_2)=\frac{4\pi}{k_ir_1r_2}P_{n_il_i}(r_1)Y^{m_i}_{l_i}(\hat{\boldsymbol{r}}_1)\sum_l\mathrm{i}^l\hat{j}_l(k_ir_2)Y^0_l(\hat{\boldsymbol{r}}_2)Y^0_l(\hat{\boldsymbol{k}}_i) \tag{20}$$

has been anti/symmetrized (depending on the spin) to account for the indistinguishability of the two electrons and thus for electron exchange. Without loss of generality we also assume the projectile to arrive along the z direction, so that its angular momentum projection to the z axis is zero. It also means that the projection of the total angular momentum is exactly equal to the initial magnetic quantum number of the atom, $M=m_i$, both before and after the collision. For this reason M is often omitted in the further expressions.

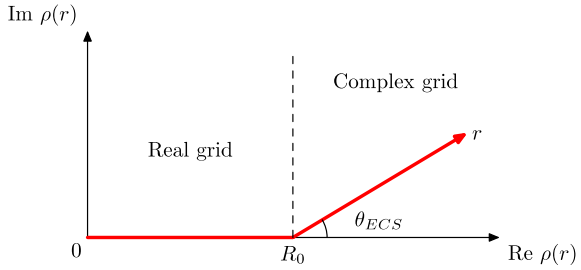

Fig. 1. ECS coordinate transformation. The original real radial coordinate r is transformed to a complex contour $\rho(r)$. In the case of hex-ecs both radial coordinates are complexified in this way.

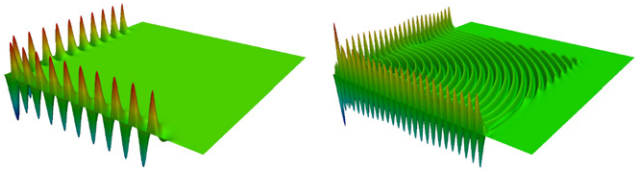

Fig. 2. The function $\psi^{000}_{00}(r_1,r_2)$ for the energies 0.6 Ry (left) and 4 Ry (right). The fast exponential damping of the wave function beyond the R_0 rotation radius can be observed. In this case R_0 is approximately in four fifths of the radial grid length.

In our approach the equations for the partial wave $\psi^{LMS\Pi}_{\rm sc}$ are not explicitly accompanied by a boundary condition. Instead, the difficulties of matching the asymptotic scattering wave are avoided by the method of *exterior complex scaling* [7] (referred to as "ECS" in the further text). The ECS is a complexification of the real radial coordinates by a rotation of the coordinate in the complex plane. Up to some distance R_0 the coordinate is kept real, larger radii are transformed by the mapping

$$r\mapsto\rho(r)=\begin{cases}r & [r<R_0]\\ R_0+(r-R_0)\mathrm{e}^{\mathrm{i}\theta_{ECS}} & [r>R_0].\end{cases} \tag{21}$$

This process is graphically represented in the well-known Fig. 1. The reason for the complex rotation is that the sought solutions should contain an outgoing wave factor $\mathrm{e}^{+\mathrm{i}kr}$; cf. Eqs. (5), (6) and (8). For $\theta_{ECS}>0$ the scattered wave will be exponentially damped in the complex region of the coordinates. Thus, the requirement (boundary condition) for the asymptotic scattering form can be recast into a zero boundary condition at some far distance $R_{\max}$, provided that $R_{\max}$ is sufficiently distant to enable damping of the expected solution to the numerical zero. The mathematical problem then simplifies to solving a set of two-dimensional differential equations with Dirichlet condition at origin and at the outer boundary; cf. the Fig. 2.

Extraction of the scattering variables is being done using the formula for the T-matrix

$$T^S=\left\langle\Psi_f\right|\hat{H}_{\rm int}\left|\Psi^S_{\rm sc}\right\rangle=\sum_{L\ell}T^{LS}_\ell Y^{m_i-m_f}_\ell. \tag{22}$$

This expression is valid only for the real coordinates, i.e. in the limit $R_0\to\infty$. The interaction part of the hamiltonian has been truncated at R_0. If we further use the equation $(\hat{H}_{\rm full}-\hat{H}_{\rm int}-E)\Psi^S_f=0$ for the asymptotic final state

$$\Psi_f(\boldsymbol{r}_1,\boldsymbol{r}_2)=\frac{4\pi}{k_fr_1r_2}P_{n_fl_f}(r_1)Y^{m_f}_{l_f}\times(\hat{\boldsymbol{r}}_1)\sum_{lm}\mathrm{i}^l\hat{j}_l(k_fr_2)Y^m_l(\hat{\boldsymbol{r}}_2)Y^m_l(\hat{\boldsymbol{k}}_f) \tag{23}$$

we arrive at

$$T_l^{LS} = \frac{1}{\sqrt{2}}\frac{4\pi}{k_f} \mathrm{i}^{-l} C^{Lm_i}_{l_f m_f l m_i - m_f} \left(\Lambda_l^{(1)Lm_iS} + \Lambda_l^{(2)Lm_iS} \right), \tag{24}$$

$$\Lambda_l^{(1)LMS} = \lim_{R_0\to\infty} \int_0^{R_0} P_{n_f l_f}(r_1)\, \mathcal{W}\left[\psi^{LMS}_{l_f l}(r_1, \bullet), \hat{j}_l(k_f \bullet) \right]_{R_0} \mathrm{d}r_1, \tag{25}$$

$$\Lambda_l^{(2)LMS} = \lim_{R_0\to\infty} \int_0^{R_0} \hat{j}_l(k_f r_2)\, \mathcal{W}\left[\psi^{LMS}_{l_f l}(\bullet, r_2), P_{n_f l_f}(\bullet) \right]_{R_0} \mathrm{d}r_2 \tag{26}$$

where $\mathcal{W}[a, b]_{x_0} = a'(x_0)b(x_0) - a(x_0)b'(x_0)$ is the Wronskian of the two functions, here with respect to the variable replaced by a bullet symbol. The second contribution $\Lambda_l^{(2)LMS}$ is negligible because both the hydrogenic function $P_{n_f l_f}$ and its derivative should be almost zero at R_0.

Hex-ecs does extract the ionization amplitude as well, using the method of the Peterkop integral [8]. Whereas the integration in (25) and (26) runs along one of the two far edges of the real section of the bi-radial (r_1, r_2) plane, which is in accordance with the assumption that only one of the electrons escapes to the continuum, in the case of ionization the extraction has to be done in a more symmetrical way—along a quarter-circle contour far from the origin in the coordinate plane. This is easy to express in the hyperspherical coordinates

$$R = \sqrt{r_1^2 + r_2^2}, \qquad \alpha = \arctan \frac{r_2}{r_1}. \tag{27}$$

In the hyperspherical coordinates the extraction contour has the form $R = \rho = \text{const}, \alpha \in \langle 0, \pi/2 \rangle$. The expression valid for asymptotic $\rho \to \infty$ then reads

$$F^S(\boldsymbol{k}_1, \boldsymbol{k}_2) = \sum_{\ell_1\ell_2 LM} \mathrm{i}^{-\ell_1-\ell_2} \mathrm{e}^{\mathrm{i}(\sigma_1+\sigma_2)} \mathcal{Y}^{LM}_{\ell_1\ell_2}(\hat{\boldsymbol{k}}_1, \hat{\boldsymbol{k}}_2) f^{LMS}_{\ell_1\ell_2}(k_1, k_2), \tag{28}$$

where

$$f^{LMS}_{\ell_1\ell_2}(k_1, k_2) = \frac{2}{\sqrt{\pi}} \frac{\rho}{k_1 k_2} \int_0^{\pi/2} \left(\phi_1\phi_2 \frac{\partial}{\partial\rho} \psi^{LMS}_{\ell_1\ell_2} - \psi^{LMS}_{\ell_1\ell_2} \frac{\partial}{\partial\rho} \phi_1\phi_2 \right) \mathrm{d}\alpha. \tag{29}$$

The newly introduced symbols $\sigma_j \equiv \sigma_{\ell_j}(k_j)$ stand for the Coulomb phase shifts and $\phi_j \equiv \phi_{\ell_j}(k_j, r_j)$ for the Coulomb partial wave functions, which are the terms of the partial wave expansion of the Coulomb wave (7).

3. Numerical solution

Whereas the outgoing complex exponential is damped if sufficiently far in the complex region, the incoming waves in the decomposition of the initial wave function (20) diverge under the transformation (21). This difficulty can be tracked up to the right hand sides of (18) and (19). To avoid the divergence, the potentials V_1, V_2 and V_{12} are usually set to zero just after R_0. Because a sharp termination of the potentials would result in reflections, some smooth weight factor has to be employed. In hex-ecs it is represented by the factor $\xi(r)$ proportional to a hyperbolic tangent that has the node shortly after R_0. Then

$$V_i'(r_i) = \xi(r_i) V_i(r_i), \qquad V_{12}'(\boldsymbol{r}_1, \boldsymbol{r}_2) = \xi(r_>) V_{12}(\boldsymbol{r}_1, \boldsymbol{r}_2). \tag{30}$$

Eq. (11) is solved in the basis of B-splines, which are already an established tool in the atomic physics [9]. The B-splines are polynomial functions of a given order with a compact support and they are illustrated in Fig. 3. The compactness brings sparsity into the matrices created by projecting equations on this basis and, moreover, the sparsity level can be adjusted by changing their order. An overlap matrix of the basis will have $2n + 1$ diagonals,

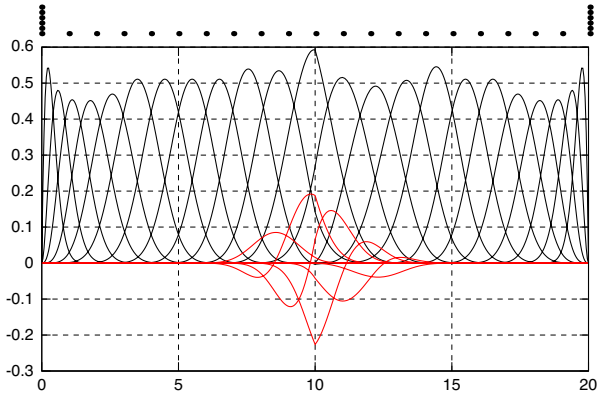

Fig. 3. B-spline set of order $n = 6$ and equidistant knots from 0 to 20, with multiplicities shown above the plot. The set has been constructed on an ECS contour rotated by $\theta_{\mathrm{ECS}} = \pi/5$ with $R_0 = 10$. Black curves are the real parts of the B-spline and red curves the imaginary parts. Note the sharp features at R_0. Also note that only such B-splines whose support includes R_0 are complex; all other B-splines are real. (For interpretation of the references to color in this figure legend, the reader is referred to the web version of this article.)

where n is the B-spline order. Combination of B-splines with the ECS is easy due to the fact that the B-splines can be defined by the order and a set of knots $\{t_i\}_{i=0}^N$ on the radial grid only, by the Cox–de Boor recursion formula [10,11]

$$B_i^{(0)}(r) = \begin{cases} 1 & t_i \le r \le t_{i+1} \\ 0 & \text{else,} \end{cases} \tag{31}$$

$$B_i^{(k)}(r) = \frac{r - t_i}{r_{i+k} - t_i} B_i^{(k-1)}(r) + \frac{t_{i+k+1} - r}{t_{i+k+1} - t_{i+1}} B_{i+1}^{(k-1)}(r). \tag{32}$$

When these knots are taken from the rotated ECS contour, the basis will be without modification compatible with the new coordinates, i.e. it will naturally contain the discontinuity at R_0, so that no special considerations are necessary there. Multiplicity of the knots influences density of the B-splines. Maximal allowed multiplicity is $n + 1$. If only n (or less) is used as the multiplicity at the origin and the end, then none of the basis elements will be nonzero there, which promptly enforces the zero Dirichlet boundary condition. The B-splines are normalized, $\sum_i B_i(x) = 1$, and a derivative of a B-spline is again a combination of B-splines,

$$\frac{\mathrm{d}B_i^{(k)}(r)}{\mathrm{d}r} = \frac{k}{t_{i+k} - t_i} B_i^{(k-1)}(r) - \frac{k}{t_{i+k+1} - t_{i+k}} B_{i+1}^{(k-1)}(r). \tag{33}$$

Being polynomials, the B-splines can be effectively integrated by the Gauss–Legendre quadrature. The N-point Gauss–Legendre rule can integrate accurately polynomials up to the degree of $2N + 1$. A product of two B-splines of order n has a degree of $2n$, so the n-point rule is sufficient. Integral moments

$$M_{ik}^{(\alpha)} = \langle B_i | \, r^\alpha \, | B_k \rangle \tag{34}$$

with a positive exponent raise this number only by $\alpha/2$. This does not hold for $\alpha < 0$, which is an equally important ingredient for the computation. It is assumed that the integrand in this case still closely resembles a polynomial, even in the $r \to 0$ limit (thanks to the zero boundary condition), and that simple addition of more integration points leads to a satisfactory result.

Beside the moment (34), which is necessary for the evaluation of both the diagonal blocks of (11) and the right hand side, one also needs the two-electron integrals

$$R^\lambda_{ijkl} = \left\langle B_i(r_1) B_j(r_2) \left| \frac{r_<^\lambda}{r_>^{\lambda+1}} \right| B_k(r_1) B_l(r_2) \right\rangle, \tag{35}$$

that serve for the evaluation of the matrix elements of V_{12} and of the right-hand side of (11). This could be a bottleneck of the computation, as there is N^4 double integrations to do, where N is the number of basis B-splines. Fortunately, the elements R^{λ}_{ijkl} have several symmetries,

(1) $R^{\lambda}_{ijkl} = R^{\lambda}_{kjil}$,

(2) $R^{\lambda}_{ijkl} = R^{\lambda}_{ilkj}$,

(3) $R^{\lambda}_{ijkl} = R^{\lambda}_{jilk}$

and their combinations (altogether six symmetries), which can speed up the calculation. Only $|i-k| \leq n$ and $|j-l| \leq n$ give nonzero integrals, thanks to the compactness. We end with circa $(2n+1)^2N^2/6$ nonzero elements per λ. Most of them are also easily computable: For $i \neq k$ and $j \neq l$ the double integral separates into a product of integral moments $M^{(\lambda)}$ and $M^{(-\lambda-1)}$.

The remaining B-spline matrix element is the kinetic energy term. Due to the fact that all B-splines decrease to zero the integration per parts transforms the second derivative into the following integral with no boundary terms:

$$D_{ik} = \langle B_i(r)| \left(-\frac{\mathrm{d}^2}{\mathrm{d}r^2}\right) |B_k(r)\rangle = + \int \frac{\mathrm{d}B_i(r)}{\mathrm{d}r} \frac{\mathrm{d}B_k(r)}{\mathrm{d}r} \mathrm{d}r. \tag{36}$$

According to (33), the integrand in (36) is again a polynomial, now of the degree $2(n-1)$.

To express the right-hand side of (17) in the language of the B-splines it is necessary to expand the initial atomic radial function $P_{n_i l_i}(r)$ and the initial projectile partial wave radial function $\hat{j}_l(k_i r)$ in the B-spline basis. This is done by the computation of overlaps

$$\mathrm{J}_a = \int B_a(r)\hat{j}_l(k_i r)\mathrm{d}r, \qquad \mathit{\Pi}_a = \int B_a(r) P_{n_i l_i}(r)\mathrm{d}r \tag{37}$$

and by solving two sets of linear equations for the components $[\hat{j}_{lk_i}]_b$ and $[P_{n_i l_i}]_b$

$$S_{ab}[\hat{j}_{lk_i}]_b = \mathrm{J}_a, \qquad S_{ab}[P_{n_i l_i}]_b = \mathit{\Pi}_a \tag{38}$$

where $S_{ab} = \langle B_a|B_b\rangle$ is the overlap matrix of the basis.

The main computation part then for all requested initial states constructs a right-hand side of (17) and executes preconditioned conjugate gradients solver. The full matrix of the set of equations is never explicitly constructed as it would be too huge and there is actually no benefit of having it. Instead, the conjugate gradients algorithm as described in [12] needs only matrix multiplication, which is easy to compute per individual blocks. The blocks are composed of sums and Kronecker products of basic matrices S, $\mathsf{M}^{(\alpha)}$, D and R^{λ} presented earlier, which may be stored in the main memory without considerable requirements on its size.

For larger grids (and resulting matrices) the iterative method has to be aided by a preconditioner. Hex-ecs contains several preconditioners, their list and short descriptions can be retrieved by running

```
> hex-ecs -P
```

and one of the implemented preconditioners can then be selected for computation by

```
> hex-ecs -p <preconditioner>
```

The default, fastest and most robust of them is the drop-tolerance incomplete LU factorization of the diagonal blocks. These are the sections of the matrix of the set of equations that conserve the angular momentum of each electron (they do not couple different angular momentum states). Preconditioning is done by applying (approximately) inverse diagonal blocks on the respective segments of the iterated right-hand side. The sparse algebra computer package SuiteSparse is used to compute the factorization, particularly its library UMFPACK [13]. Together with another free library OpenBLAS [14]implementing optimized dense linear algebra kernels the factorizations can run in multiple threads with a very good scaling.

For a quick checking of the results the program outputs cross sections in a format suitable for direct plotting by Gnuplot. But the main results are the T-matrices in the form of SQL statements, that are used to update a scattering database. This database can then be accessed using an accompanying interface code which is intended as the back end for a web interface: the hex-db program. It uses the well-spread SQL standard as provided by SQLite [15] for the data storage, so that the contents of the database can be efficiently managed by custom scripting whenever the provided interface would lack desired features. For more info on hex-db see the first article of the series.

4. Program input and output

The input data for the program hex-ecs have to be specified by a text file, by default called `hex.inp`. If using a different name, one has to tell the program the correct name using the `--input` switch. The file is unstructured, i.e. the entries do not have a specific position in the file, only a fixed order in which they appear. Lines beginning with the symbol "#" are comments. The following item list describes the entries. Every item is accompanied by a reference to the input file from the test run in Appendix A (lines 14–39), with the explanation of the entries given there.

- Order of the B-splines (line 16: fourth order).
- ECS angle in radians (line 16: $\theta_{\mathrm{ECS}} = 0.63$).
- Sequence of real knots as three sets of numbers: (a) starting points of uniformly sampled intervals and "−1" denoting end of the starting points sequence, (b) end points of the intervals, (c) number of uniform samples including the starting and end points. The last two sets are not terminated by "−1" as their count is already known—to be equal to the length of the first set. The first knot should be zero with multiplicity equal to the order, the last knot should be equal to R_0, which is the ECS rotation point. This and all other coordinates are expected in atomic units, i.e. Bohr radii a_0 (lines 18–20: real knot sequence 0.0 (4×), 0.1, 0.2, …, 1.9, 2, 3, 4, …, 79, 80).
- Sequence of the complex-to-become knots. The first knot ought to match the last real knot; the last knot should equal $R_{\max}$ (lines 22–24: sequence 80, 81, …, 119, 120).
- Initial atomic principal quantum number (line 26: $n_i = 1$).
- Initial atomic angular quantum numbers. The program can handle several initial states at one run, but only with the same energy. The angular numbers l_i and m_i are then specified in the same fashion as the knot sequences, i.e. (a) the l_i values followed by "−1" and (b) the value m_i for every l_i. Optionally, if any m_i is set to the wildcard symbol "*", all values of m_i allowed by the corresponding l_i will be used (lines 27 and 28: just one state with $l_i = m_i = 0$).
- Final atomic states. Here only n_f and l_f are to be given, because the computation of T-matrices for different m_f does not involve further solving of the equations and is done automatically. So n_f and l_f are given, again, in the same manner as the knot sequences. The wildcard symbol "*" can be used now in place of l_f if all values of l_f are to be computed for the corresponding n_f (lines 30 and 31: just one state with $n_f = 1, l_f = 0$).
- Total angular momentum L, total spin S and parity $\mathit{\Pi}$ (line 33: L and S are being set by the script, $\mathit{\Pi}$ is always zero, because only $\mathit{\Pi} = 0$ contributes to elastic scattering H(1s)→H(1s)).
- Electron angular momentum limit n_L, see the Eq. (13) (line 33: $n_L = 4$).
- Projectile energies E_i in Rydberg units in the format (a) starting energies of uniformly sampled intervals, "−1", (b) last energy

of the interval and (c) sample counts including the starting and end points (lines 35–37: only one item with $E = 4$ Ry $= 2$ a.u.).
- Third component of a uniform (weak) magnetic field in atomic units. This is included in the computation only as a first-order perturbation effect: the change of the magnetic energy of the atomic electron, $\Delta E = (m_f - m_i)B_z$, is added to the energy of the outgoing scattered electron (line 39: $B_z = 0$ a.u.).

The program hex-ecs outputs – apart from some progress information – also several text files. One group is named `sigma-`n_i-l_i-m_i-n_f-l_f-m_f-L-S `.dat` and contains integral cross section for this particular LS partial wave. Its purpose is mostly for diagnosis and convergence checking. The other is named n_i-L`.sql` and contains SQL statements to be imported into the hex-db database, typically

```
BEGIN TRANSACTION;
INSERT OR REPLACE INTO "tmat" VALUES (1,0,0, 1,0,0, 0,0, 4.0e+00, 0,
                                                          4.6,3.5, 0.0,0.0);
INSERT OR REPLACE INTO "tmat" VALUES (1,0,0, 1,0,0, 0,1, 4.0e+00, 0,
                                                          6.3,5.2, 0.0,0.0);
COMMIT;
```

The data inserted are: n_i, l_i, m_i, n_f, l_f, m_f, L, S, E_i, l, Re $T_l^{Lm_iS}$, Im $T_l^{Lm_iS}$, Re $T_{l,\mathrm{Born}}^{Lm_iS}$ and Im $T_{l,\mathrm{Born}}^{Lm_iS}$. The last two entries are the approximate Born T-matrices which, if present, are used in the Born subtraction procedure; see the first article of this series for details.

In the case of ionization, a simple T-matrix element is not sufficient to hold all information. Instead, the whole function $f_{\ell_1\ell_2}^{LMS}(k_1, k_2)$ defined in (29) is needed. This function is one-dimensional if we assume the energy conservation $k_1^2 + k_2^2 = 2E_i - n_i^{-2}$, which is asymptotically valid in the infinite proton mass approximation. The radial amplitude $f_{\ell_1\ell_2}^{LMS}(k_1, k_2)$ is rather oscillatory. In the Hex package it is stored as a Chebyshev expansion [4]

$$f_{\ell_1\ell_2}^{LMS}(k_1(x), k_2(x)) = \frac{c_0}{2} + \sum_{k=1}^{N} c_k T_k(x), \tag{39}$$

$$k_1(x) = k_{\max} x, \qquad k_2(x) = k_{\max}\sqrt{1-x^2}, \quad k_{\max} = \sqrt{2E_i - \frac{1}{n_i^2}},$$

that contains enough terms, "enough" meaning that the last of the Chebyshev coefficients (c_N) contributes by a given fraction (e.g. 10^{-10}) to the sum of absolute values of the others. The array of coefficients is then stored, byte after byte, in the raw hexadecimal format as an SQL *blob*, like in the following listing:

```
BEGIN TRANSACTION;
INSERT OR REPLACE INTO "ionf" VALUES (1,0,0, 0,0, 4.000000e+00, 0,0,
                                                    x'a46a54ff64fa65...');
INSERT OR REPLACE INTO "ionf" VALUES (1,0,0, 0,1, 4.000000e+00, 0,0,
                                                    x'10af32fa54faf6...');
COMMIT;
```

The data inserted are: n_i, l_i, m_i, L, S, E_i, ℓ_1, ℓ_2 and $\{c_k\}_{k=0}^{N}$.

5. Results

The validity of the exterior complex scaling method has been already convincingly demonstrated in several articles [2,16,7]. This section contains results from several computations that verify the presented computer code. Comparison is done with the data from Aladdin database [17] and with the available experimental data.

The low-energy elastic scattering is the most easily computable process; the ground state of hydrogen does not span a large space in contrast to the excited states and a small spatial basis reaching not much further than 100 atomic units is mostly sufficient. The number of partial waves necessary to obtain a result converged to within 1% is small, typically less than ten, except for high-partial-wave resonances. An example of such computation is presented in Fig. 4.

While increasing the impact energy, the partial wave count rises, too, and the spatial basis needs refinement to allow description of the rapidly oscillating wave functions. Fig. 5 demonstrates the increase of influence of higher partial waves towards higher energies. The evaluation of the differential cross section, ionization cross section and electron–photon correlation coefficients requires even more partial waves, as these quantities make use of the T-matrix phase, besides its modulus. The composition of phases converges much more slowly than the simple sum of absolute values squared. This is illustrated in Figs. 6–8, respectively. Particularly in the case of ionization the amplitudes may, for some combination of electron momenta, oscillate regardless of the extraction distance

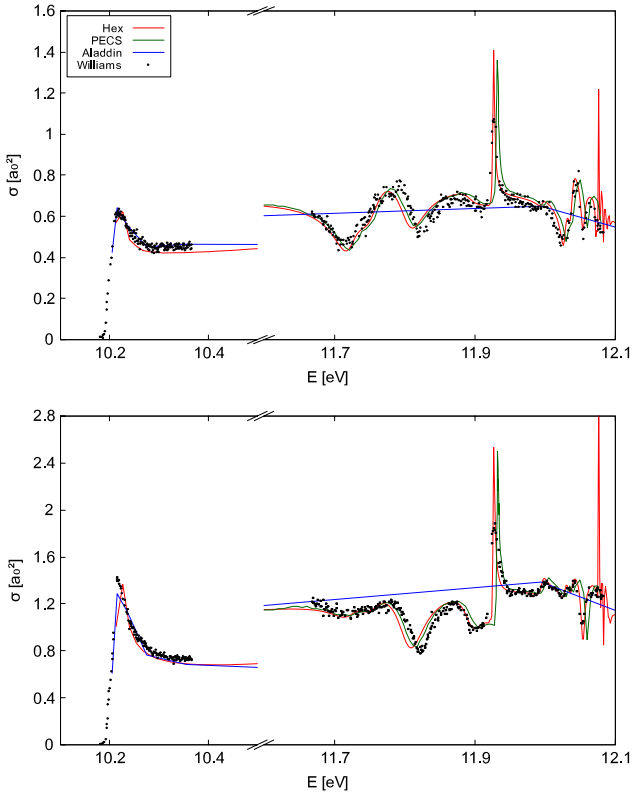

Fig. 4. The integral cross section for the excitation from the ground state H(1s) to states H(2s) (top) and H(2p) (bottom), labeled "Hex". The experimental points come from the measurement of Williams [19] and the other data from the database Aladdin (computation by Bray & Stelbovics [17] using converged close coupling) and from the computation of Bartlett [2] using the propagating exterior complex scaling (labeled PECS).

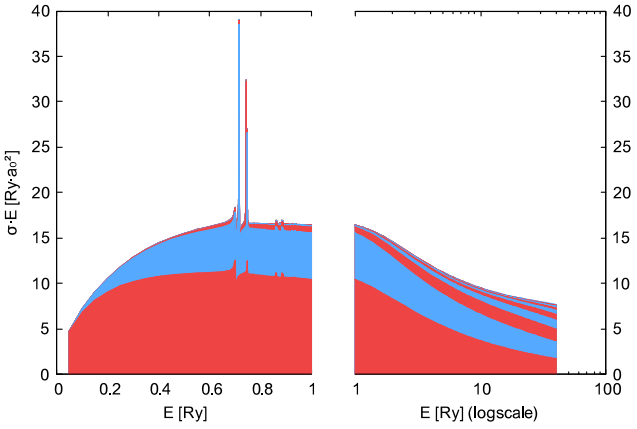

Fig. 5. Contribution of different partial waves to the complete integral cross section of the elastic scattering on H(1s) starting from $L = 0$ (bottom red) up to $L = 9$ (top blue). (For interpretation of the references to color in this figure legend, the reader is referred to the web version of this article.)

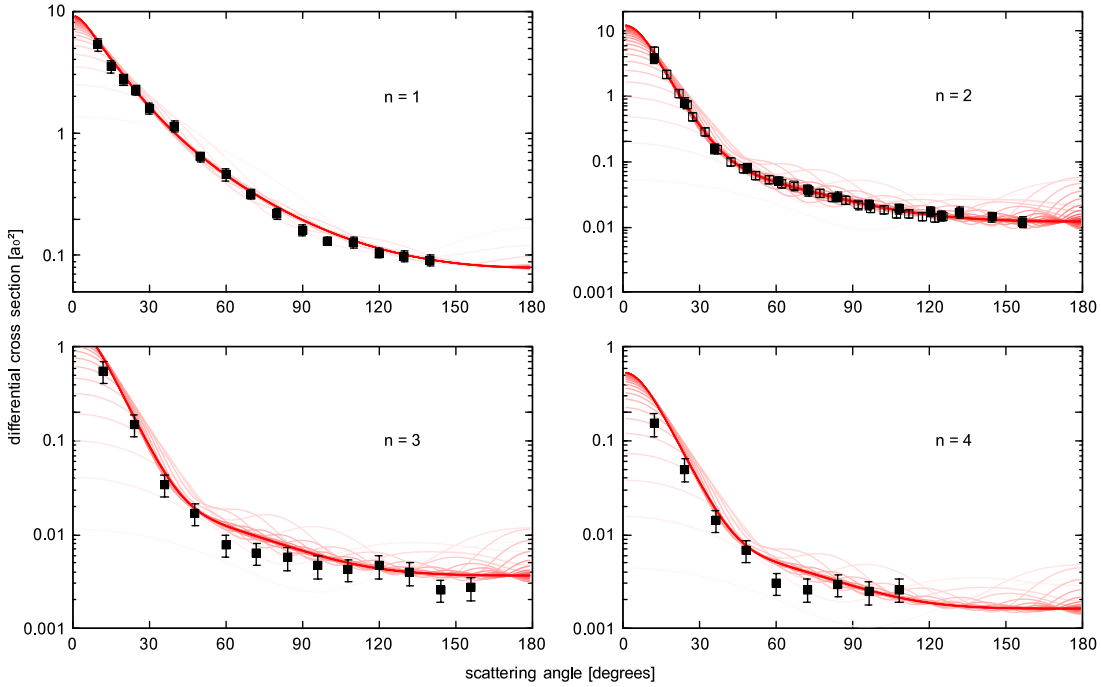

Fig. 6. The summed differential cross sections for transitions from the ground state to $n = 1, 2, 3$ and 4 levels at the impact energy $E = 30$ eV. The experimental data are taken from [20] ($n = 1$), [21,22] ($n = 2$) and [23] ($n = 3, 4$). The convergence with respect to the partial wave count is shown using the gradation of saturation. The converged results correspond to approximately 25 partial waves.

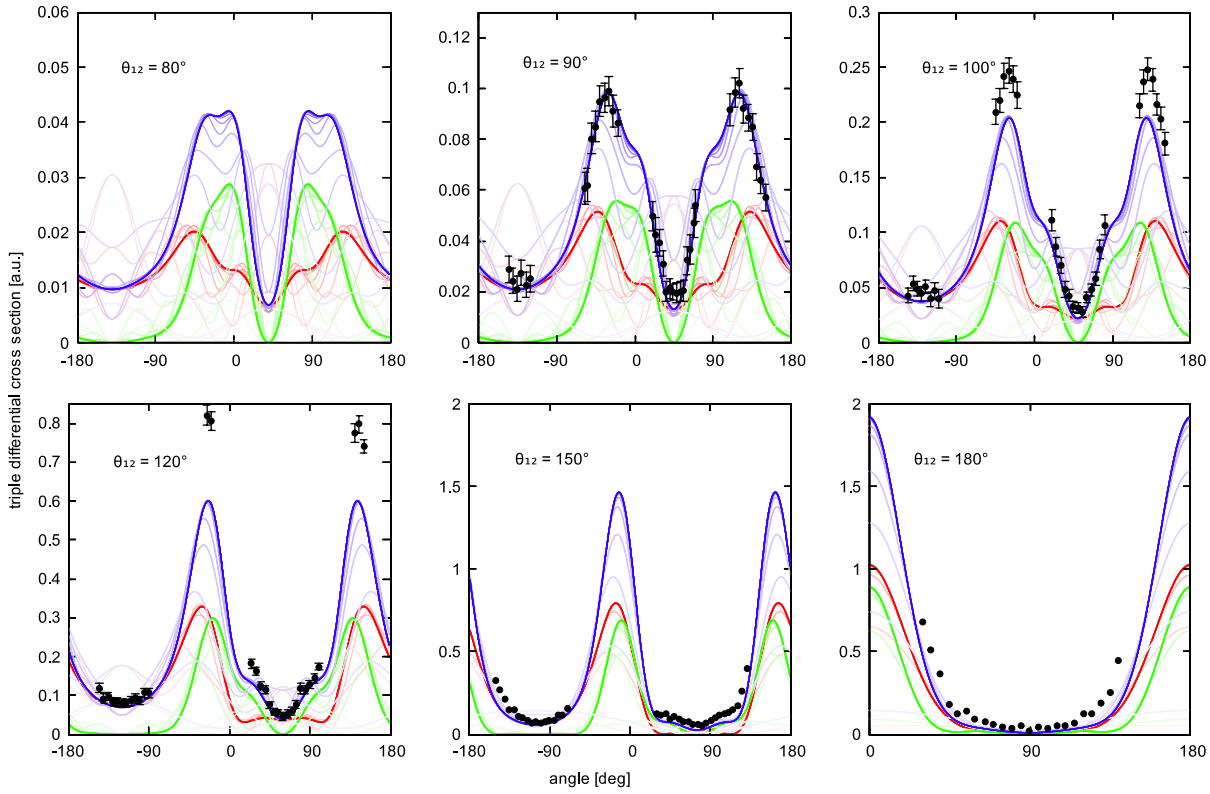

Fig. 7. The coplanar equal energy sharing triple differential cross section for the ionization of the ground state H(1s) at the impact energy $E = 17.6$ eV and for different outgoing angles of the electrons. Red curves show the singlet contribution ($S = 0$), green curves the triplet ($S = 1$) and blue curves the sum. The convergence with respect to the partial wave count is shown using the gradation of saturation. The converged results correspond to approximately 15 partial waves. (For interpretation of the references to color in this figure legend, the reader is referred to the web version of this article.)
Source: The experimental data are taken from [24].

used, unless a more sophisticated form of extraction formula is used. A recent article by Kadyrov et al. [18] presents such a formula. For discrete transitions the Born T-matrices produced e.g. by the intermediate-energy module hex-pwba2 (to be published as the third article of this series) can be used to accelerate the convergence of the partial wave series by the Born subtraction method.

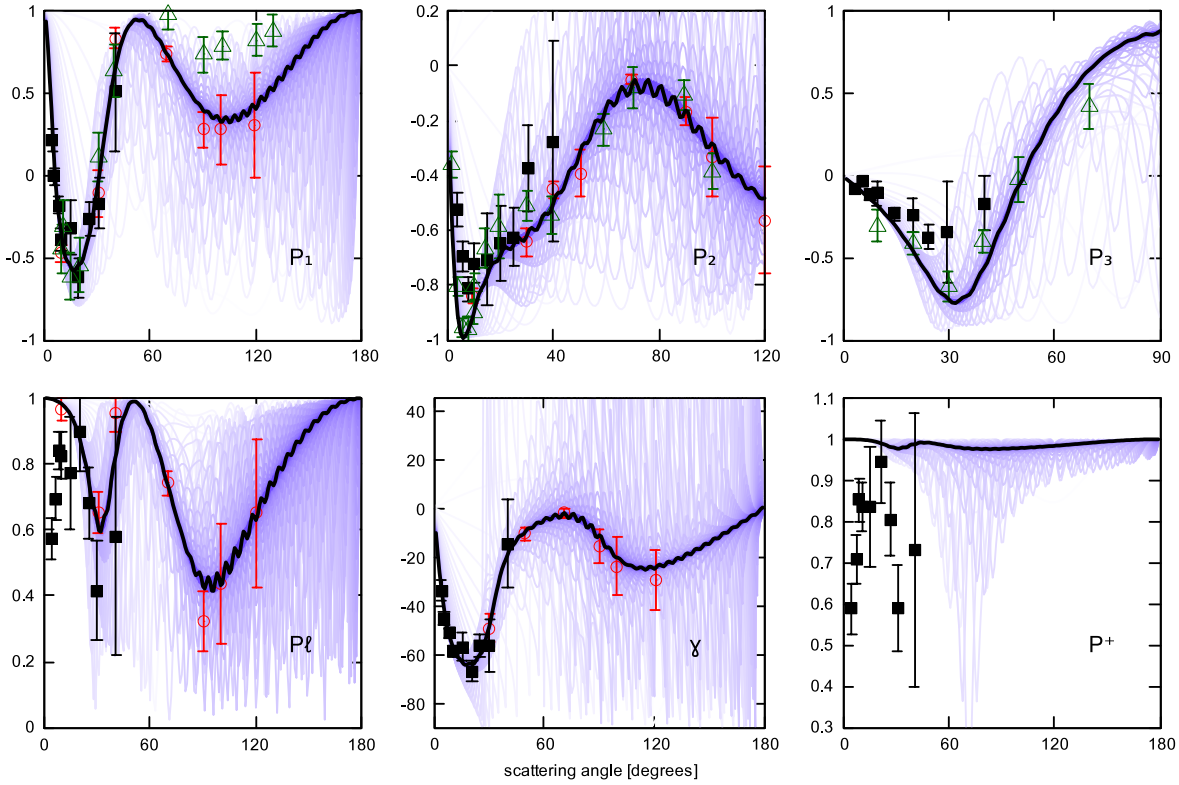

Fig. 8. The reduced Stokes parameter vector $\boldsymbol{P}$ and derived variables P_l, γ and P^+ for the transition H(1s) to H(2p) at the impact energy $E = 54.4$ eV compared with the experiments [25] (open red circles), [26] (black boxes) and [27] (green triangles). The convergence with respect to the partial wave count is shown using the gradation of saturation. The result of summing 70 partial waves is outlined by a stronger black curve. Apparently, the computation would need more partial waves to fully converge.

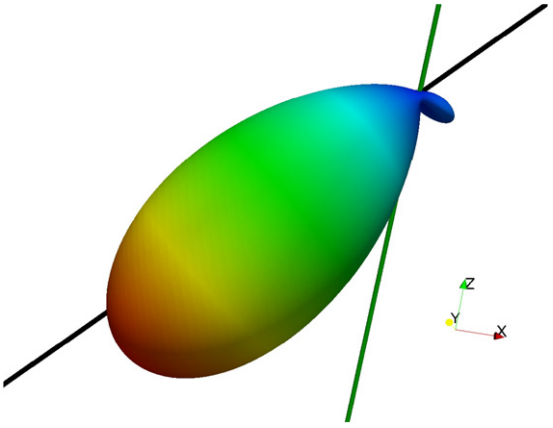

Fig. 9. Equal energy sharing triple differential cross section 3-D plot for the ionization of the ground state H(1s) at the impact energy $E = 17.6$ eV and for the scattering angle $\vartheta_1 = 45°$ of one of the electrons. The coordinate system is aligned to the outgoing direction of that electron (green z axis) and the other axis that lies in the scattering plane is the x axis. The black line is the impact direction and hence lies in the xz plane as well. The large *binary* peak of the second electron is oriented mostly in the opposite direction with respect to the first electron. The small *recoil* peak is oriented approximately perpendicular to the direction of the first electron. (For interpretation of the references to color in this figure legend, the reader is referred to the web version of this article.)

Fig. 9 shows a complete 3-D triple differential cross section diagram. The script that has been used for its construction is shown in Appendix B.

6. Conclusion

We have created a free implementation of the exterior complex scaling method for the solution of the electron–hydrogen scattering (non-relativistic, at the moment). The presented program hex-ecs is a part of the larger program package Hex that is intended to enable computation of scattering cross sections and other quantities for various electron–hydrogen processes. The expected audience are the applied atomic physics fields, like the plasma physics or the physics of the stellar atmospheres. With this in mind, a particular emphasis has been put to the simplicity of the interface to allow a straightforward usage.

The computation module hex-ecs solves the two-electron Schrödinger equation and produces intermediate computational results (partial T-matrices) that are being aggregated in the common storage, which is a SQLite database. Other modules have been presented in the first article of this series and others are in development. We also plan to include the relativistic effects in Hex to account for the astrophysically interesting transitions in the fine structure.

The user interface module hex-db accesses the intermediate database and can be used to generate required scattering quantities (various amplitudes, cross sections and other statistics) from the basic data acquired by the computational modules.

Acknowledgments

The work was supported by the Charles University in Prague, project GA UK No 730214, and by grant SVV-260089.

The access to computing and storage facilities owned by parties and projects contributing to the National Grid Infrastructure MetaCentrum, provided under the programme "Projects of Large Infrastructure for Research, Development, and Innovations" (LM2010005) is greatly appreciated. Also, the access to the CERIT-SC computing and storage facilities provided under the programme Center CERIT Scientific Cloud, part of the Operational Program Research and Development for Innovations, reg. no. CZ. 1.05/3.2.00/08.0144 is greatly appreciated.

Appendix A. Test run

The test run computes the differential elastic cross section of the electron incident on the hydrogen atom in the ground state, at the impact energy $E_i = 4\,\mathrm{Ry} = 54.4$ eV. The radial grid extends to $R_{\max} = 120a_0$ with $R_0 = 80a_0$. Knots are spaced by $1a_0$ except for a region near to the origin, where the spacing is ten times finer. Angular momenta of the electrons are restricted to $\ell \leq 4$ and the total angular momenta L range from 0 to 3.

A listing of the script that runs the sequence follows. For every partial wave L a new configuration file is created and the computations (hex-ecs) are sequentially launched. After the computations are done, the SQL database is created using the interface program hex-db and the differential cross sections are extracted into the text files `singlet.dcs` and `triplet.dcs` in the format ready for visualization in Gnuplot. It is assumed that both hex-ecs and hex-db are in the executable path. The resulting plot is shown in Fig. A.10.

```
#!/bin/bash

# limit CPU usage to 4 threads
export OMP_NUM_THREADS=4

# create new database
rm -f hex.db
hex-db --new

# compute the T-matrices using hex-ecs
for L in 0 1 2 3; do
for S in 0 1; do
    cat > hex.inp <<-EOF
    # B-spline parameters
    # order     theta
         4      0.63
    # real knot sequences
        0  0.1    3   -1
        0  2.0   80
        4   20   78
    # complex knot sequences
        80   -1
       120
        41
    # initial atomic state
       1
       0 -1
       *
    # final atomic states
       1 -1
       *
    # angular momenta (L, S, Pi, limit)
       $L  $S  0  4
    # initial energies in Rydbergs
       4   -1
       4
       1
    # magnetic field
       0
EOF
    hex-ecs | tee hex-L$L-S$S.log
    hex-db --import 1-$L-$S-0.sql
done
done

hex-db --update

# extract differential cross sections using hex-db
seq 1 179 | hex-db --dcs \
    --ni=1 --li=0 --mi=0 \
    --nf=1 --lf=0 --mf=0 \
    --Ei=4 --S=0 > singlet.dcs
```

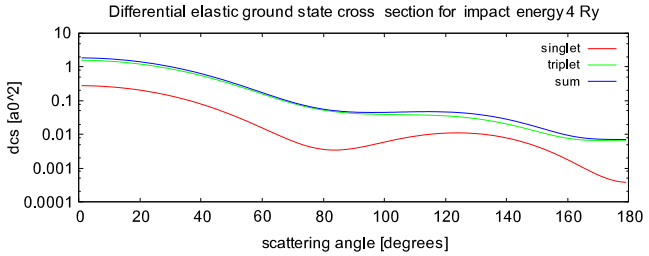

Fig. A.10. The test run output. For the above settings, the differential cross section is not yet converged—more partial waves would be needed to obtain a smooth curve without oscillations.

```
seq 1 179 | hex-db --dcs \
    --ni=1 --li=0 --mi=0 \
    --nf=1 --lf=0 --mf=0 \
    --Ei=4 --S=1 > triplet.dcs

# show graphics
gnuplot <<EOF
set title "Differential cross section"
set xlabel "scattering angle [degrees]"
set ylabel "dcs [a{0}^{2}]"
set logscale y
plot "singlet.dcs" with lines title "singlet", \
     "triplet.dcs" with lines title "triplet", \
     "< paste singlet.dcs triplet.dcs" \
         using 1:(\$2+\$4) with lines title "sum"
pause mouse
EOF
```

Appendix B. Construction of the TDCS 3-D plot

The output of hex-db consists of plain column data. It is designed for work with one-dimensional functions, like the dependency of the scattering amplitude on angle, cross section on energy etc. However, the column output is unsuitable for visualization of the three-dimensional full triple differential cross section. The transformation from a table of data produced by hex-db to an OBJ model, that can be easily viewed e.g. in ParaView, can be accomplished by a simple shell script. In the following listing an example of such script is presented. It has been used to create the Fig. 9.

```
#!/bin/bash

# create file containing evaluation directions
rm -f tdcs.out dirs.inp
for theta2 in $(seq 1 179); do
for phi2 in $(seq 0 359); do
    echo "(45 0 1) ($theta2 $phi2 1)" >> dirs.inp
done
done

# launch two processes evaluating the TDCS
cat dirs.inp | hex-db --tdcs \
    --Eunits=eV --ni=1 --li=0 --mi=0 \
    --S=0 --Ei=17.6 > tdcs3D.singlet.out &
cat dirs.inp | hex-db --tdcs \
    --Eunits=eV --ni=1 --li=0 --mi=0 \
    --S=1 --Ei=17.6 > tdcs3D.triplet.out &

# wait for completition of the launched processes
for job in ‘jobs -p‘; do
    echo $job
    wait $job
done

# extract only interesting information from the output
grep -v "#" tdcs3D.singlet.out | \
    cut -f3- | awk ’{ print $2, $3, $1; }’ \
```

```
    > tdcs3D.singlet.sph
grep -v "#" tdcs3D.singlet.out | \
    cut -f3- | awk '{ print $2, $3, $1; }' \
    > tdcs3D.triplet.sph
paste tdcs3D.singlet.sph tdcs3D.triplet.sph | \
    awk '{ print $1, $2, $3 + $6; }' > tdcs3D.sph

# convert into Cartesian format and write to OBJ file
awk '{ print "v", $3*sin($1/57.29578)*cos($2/57.29578),
                $3*sin($1/57.29578)*sin($2/57.29578),
                 $3*cos($1/57.29578); }' tdcs3D.sph \
                  > tdcs3D.obj

# append quadrangle information to the OBJ file
for theta2 in $(seq 0 178); do
for phi2 in $(seq 0 359); do
    a=$(echo "$theta2*360+$phi2" | bc)
    b=$(echo "(($theta2+1)%179)*360+$phi2" | bc)
   c=$(echo "(($theta2+1)%179)*360+($phi2+1)%360" | bc)
    d=$(echo "$theta2*360+($phi2+1)%360" | bc)
    echo "f $a $b $c $d" >> tdcs3D.obj
done
done
```

References

[1] I. Bray, et al., Phys. Rep. 520 (2012) 135–174.
[2] P.L. Bartlett, J. Phys. B: At. Mol. Opt. Phys. 39 (2006) R379.
[3] M. Brauner, J.S. Briggs, H. Klar, J. Phys. B: At. Mol. Opt. Phys. 22 (1989) 2265.
[4] W.H. Press, et al., Numerical Recipes: The Art of Scientific Computing, third ed., Cambridge University Press, New York, NY, 2007.
[5] M. Abramowitz, I. Stegun, Handbook of Mathematical Functions, fifth ed., Dover, New York, 1964.
[6] A.R. Edmonds, Angular Momentum in Quantum Mechanics, Princeton University Press, Princeton, New Jersey, 1957.
[7] C.W. McCurdy, M. Baertschy, T.N. Rescigno, J. Phys. B: At. Mol. Opt. Phys. 37 (2004) R137.
[8] R.K. Peterkop, Theory of Ionization of Atoms by Electron Impact, Colorado Associated Univ. Press, Denver, CO, 1977.
[9] H. Bachau, et al., Applications of B-splines in atomic and molecular physics, Rep. Progr. Phys. 64 (2001) 1815.
[10] C. de Boor, A Practical Guide to Splines, Springer, New York, 1978.
[11] H. Prautzsch, Bézier and B-spline Techniques, Springer, New York, 2002.
[12] R. Barrett, et al., Templates for the Solution of Linear Systems: Building Blocks for Iterative Methods, second ed., SIAM, Philadelphia, PA, 1994.
[13] T.A. Davis, ACM Trans. Math. Software 30 (2004) 196–199.
[14] Z. Xianyi, W. Qian, Z. Yunquan, 2012 IEEE 18th International Conference on Parallel and Distributed Systems (ICPADS), 17–19 Dec., 2012.
[15] M. Owens, The Definitive Guide to SQLite (Definitive Guide), Apress, Berkeley, CA, 2006.
[16] C.W. McCurdy, F. Martín, J. Phys. B: At. Mol. Opt. Phys. 37 (2004) 917–936.
[17] I. Bray, A.T. Stelbovics, Adv. At. Mol. Opt. Phys. 35 (1995) 209–254.
[18] Kadyrov, et al., Phys. Rev. Lett. 91 (2003) 253202.
[19] J.F. Williams, J. Phys. B: At. Mol. Opt. Phys. 21 (1988) 2107.
[20] J.F. Williams, J. Phys. B: At. Mol. Phys. 8 (1975) 2191.
[21] A. Grafe, C.J. Sweeney, T.W. Shyn, Phys. Rev. A 63 (2001) 052715.
[22] M.A. Khakoo, et al., Phys. Rev. A 61 (1999) 012701.
[23] C.J. Sweeney, A. Grafe, T.W. Shyn, Phys. Rev. A 64 (2001) 032704.
[24] J. Röder, M. Baertchy, I. Bray, Phys. Rev. A 64 (2003) 010702(R).
[25] H.A. Yalim, D. Cvejanovic, A. Crowe, J. Phys. B: At. Mol. Opt. Phys. 32 (1999) 3437.
[26] M.L. Gradziel, R.W. O'Neill, J. Phys. B: At. Mol. Opt. Phys. 37 (2004) 1893.
[27] J.F. Williams, A.G. Mikosza, J. Phys. B: At. Mol. Opt. Phys. 39 (2006) 4113.